Reanalysis of Relativistic Radiation Belt Electron Fluxes using CRRES Satellite Data, a Radial Diffusion Model and a Kalman Filter

Yuri Shprits[1], Dmitri Kondrashov[1,2], Yue Chen[4], Richard Thorne[1], Michael Ghil[1,2,3], Reiner Friedel[4], and Geoff Reeves[4]

[1]Department of Atmospheric and Oceanic Sciences, University of California, Los Angeles, CA 90095-1565, U.S.A.

[2]Institute of Geophysics and Planetary Physics, University of California, Los Angeles, CA 90095-1567, U.S.A.

[3]D´epartement Terre-Atmosph`ere-Oc´ean and Laboratoire de M´et´eorologie Dynamique (CNRS and IPSL), Ecole Normale Sup´erieure, F-75231 Paris Cedex 05, FRANCE

[4] Los Alamos National Laboratory, Los Alamos, NM, USA

Abstract

In this study we perform a reanalysis of the sparse MEA CRRES relativistic electron data using a relatively simple 1D radial diffusion model and a Kalman filtering approach. By combining observations with the model in an optimal way we produce a high time and space resolution reanalysis of the radiation belt electron fluxes over a 50 day period starting on August 18, 1990. The results of the reanalysis clearly show pronounced peaks in the electron phase space density (PSD), which can not be explained by the variations in the outer boundary, and can only be produced by a local acceleration processes. The location of the innovation vector shows that local acceleration is most efficient at L^*=5.5 for electrons at K=0.11 $G^{0.5}$ R_E and μ=700 MeV/G. Sensitivity numerical experiments for various values of μ and K indicate that peaks in PSD become stronger with increasing K and μ. To verify that our results are not affected by the limitations of the satellite orbit and coverage we performed an "identical twin" experiments with synthetic data specified only at the locations for which CRRES observations are available. Our results indicate that the model with data assimilation can accurately reproduce the underlying structure of the PSD even when data is sparse. The identical twin experiments also indicate that PSD at particular L-shell is determined by the local processes and can not be accurately estimated unless local measurements are available.

1. Introduction

The Earth's energetic electron radiation belts exhibit a two zone structure with the inner belt being very stable and outer belt varying on the timescales ranging from minutes to weeks. There are three adiabatic invariants (μ, J, Φ), each of which is associated with one of the three periodic motions: gyro-motion, the bounce motion in the Earth's magnetic mirror field, and the azimuthal drift due to magnetic curvature and gradients. In observational studies the invariant K, which is a combination of the first and the second adiabatic invariants, is often used. Invariant K is a purely field-geometric quantity, which is independent of the particle charge and mass. Adiabatic invariants may be related to measured satellite quantities (see Appendix A).

Each invariant can be violated when the system is subject to fluctuations on time scales comparable to or shorter than the associated periodic motion [*Schulz and Lanzerotti*, 1974]. In the collisionless magnetospheric plasma, wave-particle interactions provide the dominant mechanism for violation of the invariants, leading to changes in radiation belt structure. When the PSD of radiation belt particles increases with increasing radial distance, ULF waves, violating the third adiabatic invariant Φ, provide random displacements in radial location, which lead to a net diffusive inward transport. If the first two adiabatic invariants are are conserved, inward motion of the particles into the region of stronger magnetic field results in the acceleration of particles. Since the power in ULF waves is considerably enhanced during magnetic storms [*Mathie and Mann*, 2000], radial diffusion is considered to be an important mechanism to account for the acceleration of energetic electrons during storm conditions.

Radial diffusion models [*e.g. Brautigam and Albert*, *2000; Miyoshi et al.*, *2003; Shprits et al.*, 2005], are capable of reproducing the general structure of the radiation belts and the inner boundary of fluxes by redistributing relativistic electrons. However, radial diffusion with constant outer boundary is incapable of reproducing pronounced peaks in PSD [*Shprits and Thorne,* 2004], frequently observed in the recovery phase of a storm [*Selesnick and Blake,* 2000; *Green and Kivelson,* 2004; *Iles et al.*, 2006, *Chen et al.,* 2006]. The peaks in PSD observed in these studies are consistent with local acceleration by VLF chorus waves and later redistribution by diffusion [*Varotsou et al.*, 2005; *Shprits et al.*, 2006b] but could also be explained by variations in the PSD at the outer boundary of the radiation belts, the difference in pitch-angle distributions at different L-shells, or the systematic differences in measurements on different satellites.

In this study we use a radial diffusion model and a Kalman filter [Kalman, 1960] to produce an objective analysis of the sparse PSD observed on CRRES satellite [*Vampola, et al.*, 1992] for various values of adiabatic invariants μ and K. We show that our diffusion model [Shprits et al., 2005; 2006b], without local acceleration processes, combined with observations that respond to the net effect of all processes, can identify where diffusion alone is insufficient to account for observed PSD peaks. We further use the results of this reanalysis to determine the location of the peak of fluxes and verify that the peaks are not formed by variations in the outer boundary.

2. Model and Observations

2.1 CRRES MEA Observations

In this study, we use observations of the electron PSD from the Combined Release and Radiation Effects Satellite (CRRES). CRRES was launched in July 1990 with a highly elliptical geosynchronous transfer orbit, and the mission ended in October 1991 due to a power subsystem failure. The Medium Electron A (MEA) instrument aboard CRRES measured pitch-angle resolved electron fluxes with an energy range from 110 keV to 1527 keV [*Vampola et al.*, 1992]. The low inclination of CRRES (~18^{o}) allowed the MEA instrument to measure near-equatorially mirroring electrons across a range of L-shells.

To convert the differential electron flux measured on CRRES into PSD at given phase space coordinates (*μ, K, L*), we also need magnetic field information. The in-situ magnetic field measurements from the fluxgate magnetometer aboard CRRES are used for the calculation of *μ*. A global magnetic field model is needed to calculate *K* and *L*, and here we use the *Tsyganenko* 1996 model [*Tsyganenko and Stern,* 1996]. More details on the calculation of PSD and adiabatic invariants is given in [*Chen et al.*, 2005; 2006].

In Section 2 and 3 we study PSD at fixed values of invariants μ and *K*. Equatorial pitch-angle and kinetic energy may be related to adiabatic invariants using definitions given in Appendix A. For a dipolar magnetic field, the equatorial pitch-angle of electrons may be related to the invariant *K* as [Schulz and Lanzerotti, 1974] :

$$\boldsymbol{y}\sqrt{\frac{\boldsymbol{L}}{0.31}}\boldsymbol{K} - 2.7604(1-\boldsymbol{y}) + 0.6396(\boldsymbol{y}\ln\boldsymbol{y} + 2\boldsymbol{y} - 2\sqrt{\boldsymbol{y}}) = 0 \qquad (1)$$

where y=sin(α),the invariant *K* is measured in $G^{0.5}R_E$. Kinetic energy of a particle may be related to the first adiabatic invariant as

$$\boldsymbol{E} = \boldsymbol{E}_0\left\{\sqrt{\left(\frac{2\boldsymbol{B}\boldsymbol{\mu}}{\boldsymbol{E}_0\sin^2(\alpha)}+1\right)}-1\right\} \qquad (2)$$

Figure 1 shows the variation in pitch-angle and energy of electrons at *K*=0.11 $G^{0.5}$ and μ=700 MeV/G as they radially diffuse, conserving the first two adiabatic invariants, in a dipolar magnetic field and can also be used to relate PSD at a given *L* to the more familiar quantities of pitch angle and energy. While pitch-angle of electrons changes by only few degrees, electrons can gain (or loose) a relatively large amount of kinetic energy by diffusing inwards (or outwards) by only few L-shells.

Figure 2 top shows CRRES MEA observations of PSD at K=0.11 $G^{0.5}$ R_E and μ=700 MeV/G. When PSD is inferred from the observations of fluxes at fixed kinetic energy, the restrictions in minimum and maximum energy observed by MEA results in a limited range of L-shells for which PSD is available. Since the CRRES orbit is approximately 8.5 hours the data is not available every hour and orbital properties impose limitations on the radial coverage of the inferred PSD. Consequently in the current study we combine the radial diffusion model with hourly averaged CRRES MEA observation at fixed values of K and μ by means of Kalman filtering.

At our chosen values of μ=700 MeV/G and K=0.11 $G^{0.5}$ R_E the electron kinetic energy is above 0.5 MeV and thus electrons experience a net acceleration by chorus waves [e.g. *Meredith et al.*, 2001, 2002; *Horne and Thorne*, 2003; *Horne et al*., 2005a; *Shprits et al.*, 2006a, *Li et al.*, 2007] leading to peaks in PSD. This choice of values of the adiabatic invariants also allows us to infer PSD for a relatively large range of L-shells from CRRES MEA observations.

2.2 Radial Diffusion Model

If the first and second adiabatic invariants are conserved, the violation of the third invariant may be described by the radial diffusion equation [e.g. *Shultz and Lanzerotti*, 1974]

$$\frac{\partial \boldsymbol{f}}{\partial \boldsymbol{t}} = \boldsymbol{L}^2 \left(\frac{\partial}{\partial \boldsymbol{L}} \right)_{\mu, J} \left[\boldsymbol{D}_{LL} \boldsymbol{L}^{-2} \left(\frac{\partial \boldsymbol{f}}{\partial \boldsymbol{L}} \right)_{\mu, J} \right] - \frac{\boldsymbol{f}}{\tau_L}, \quad (3)$$

where $f(L,t)$ is the particle phase-space density (PSD) at a fixed first and second adiabatic invariants, D_{LL} is the cross-L diffusion coefficient, τ_L is the time scale for particle losses.

In this study we adopt a data-derived empirical relationship for the rate of radial diffusion due to magnetic fluctuations [*Brautigam and Albert,* 2000]

$$\boldsymbol{D}_{\boldsymbol{LL}}^{\boldsymbol{M}}(\boldsymbol{Kp},\boldsymbol{L}) = 10^{(0.506\,\boldsymbol{Kp}-9.325)}\boldsymbol{L}^{10}, \boldsymbol{Kp} = 1 \ \boldsymbol{to} \ 6 \qquad (4)$$

which tends to dominate throughout the outer radiation zone. Parameterization (4) is consistent with the theoretical estimates of *Perry et al*, [2005] in the heart of the outer zone.

Figure 2 (middle) shows the results of the radial diffusion simulations. The model with constant boundary conditions does not produce significant variations in the outer region, but approximately describes the inner boundary of fluxes and the location of the peak of fluxes [*Shprits et al.*, 2005]. Our model is driven by the variation in Kp index only, which modulates both radial diffusion rates and lifetimes (Figure 2 bottom). The inner boundary for our simulation $f(L=1)=0$ is taken to represent loss to the atmosphere, while the outer boundary condition is set at L=7. To solve the radial diffusion equation we use an implicit unconditionally stable scheme. Lifetime τ_L is parameterized as 5/Kp following [Shprits et al., 2006b]. For more detailed description of the model see [*Shprits et al.*, 2005; 2006b].

3. Data Assimilation using the Kalman Filter

Data assimilation is an algorithm which allows for optimal combination of model results and sparse data from various sources, contaminated by noise and systematic errors [*Kalman*, 1960]. The accuracy of any model predication depends on the accuracy of estimation of the initial state of the system and on how well dominant physics is described by the model. At the times of updates the data assimilation filtering algorithm first verifies the model forecast with data, and then combines data with the model results.

Satellite observations are often restricted to a limited range of *L* shells, pitch-angles, and energies. Additionally observations at different L-shells are taken at different points along the spacecraft orbit and therefore at different times. The unavoidable limitations in the data complicates the analysis of the radial profiles of the PSD, which is essential for understanding the relative contribution of either local acceleration or radial transport on the evolution of the radiation belt electrons. Therefore, to understand the dynamics and dominant physical processes in the radiation belts as well as to create accurate statistical models, observations should be combined with physics based dynamical models. *Friedel et al*., [2003] assimilated geosynchronous and GPS data by directly inserting it into the Salambo code [e.g. *Bourdarie*, 1997; 2000], which solves the modified Fokker-Planck equation. More recently *Naehr and Toffoletto*, [2005] by using an idealized radial diffusion model (with no losses or sources) illustrated, using an example of synthetic data ("data" produced by the model with which has a slightly different set of parameters) how more advanced, optimal techniques (Kalman filter) may be applied to radiation belt forecasts.

The "Kalman filter" is a data assimilation method which combines a numerical model and sparse data, in a way which minimized mean-squared errors [*Kalman*, 1960]. The underlining assumption of the Kalman filter is that the errors of model and observations are unbiased and obey Gaussian distribution. The sequential Kalman filter is applied during the update times. The numerical forecast is first verified against the new data, and then combined with data. Evolution of errors is accounted for by the error covariance matrix which is propagated in time by the Kalman filter. Kalman filter also includes the possibility to constrain uncertain parameters of the physical model. Kondrashov et al. (2007) used the Kalman filter and 1 MeV electron fluxes observed on CRRES to estimate the lifetimes of relativistic electrons in a radial diffusion model. Parameter estimation is a more challenging problem than a mere state estimation due to additional nonlinearities that arise in the estimation process, and requires non-linear extensions of the standard Kalman filter formulation, outlined below.

3.1 Kalman Filtering Methodology

For a given system of the partial differential equations the numerical algorithm, explicit or implicit, may be presented in a discrete form:

$$\boldsymbol{w}_{\boldsymbol{k}}^{\boldsymbol{f}} = \Psi_{\boldsymbol{k}-1}\boldsymbol{w}_{\boldsymbol{k}-1}^{\boldsymbol{f}}, \tag{5}$$

where $\boldsymbol{w}$ represents a state vector, which is composed of all model variables (for our radiation belt model, it is a vector of PSD at various L) and Ψ is a matrix of the numerical model (in our case of discretized Eq. (4)) which advances the PSD in discrete time increments). Superscript "*f*" refers to a forecast and the subscript indicates the time step. The evolution of $\boldsymbol{w}_{\boldsymbol{k}}^{\boldsymbol{t}}$ (superscript "*t*" refers to "true") is assumed to be given by

$$\boldsymbol{w}_{\boldsymbol{k}}^{\boldsymbol{t}} = \Psi_{\boldsymbol{k}-1}\boldsymbol{w}_{\boldsymbol{k}-1}^{\boldsymbol{t}} + \boldsymbol{b}_{\boldsymbol{k}-1}^{\boldsymbol{m}} \tag{6}$$

where $\boldsymbol{b}_{\boldsymbol{k}}^{\boldsymbol{m}}$ is a model error, represented by a spatially correlated E($\boldsymbol{b}^{\boldsymbol{m}}\,\boldsymbol{b}^{\boldsymbol{m}T}$)=Q white noise (E($\boldsymbol{b}^{\boldsymbol{m}}$)=0), Q is a model covariance matrix, and symbol E represents an expectation operator in time. The observations $\boldsymbol{w}_{\boldsymbol{k}}^{\boldsymbol{o}}$ (superscript "o" refers to "observed") are assumed to be also contaminated by errors:

$$\boldsymbol{w}_{\boldsymbol{k}}^{\boldsymbol{o}} = \boldsymbol{H}_{k}\boldsymbol{w}_{\boldsymbol{k}}^{\boldsymbol{t}} + \boldsymbol{b}_{\boldsymbol{k}}^{\boldsymbol{o}} \quad (7)$$

where $\boldsymbol{b_k}^{\boldsymbol{o}}$ is an observational error, represented by a spatially correlated (E(b^o b^{oT})=R) white noise (E(b^o)=0) , R is an observational error covariance matrix.

The observational matrix H_k maps the true space on to the observed space and accounts for the fact that only certain variables are observed and the number of observed variables is usually less then the dimension of a state vector. During the update times we use the forecasted state vector and vector of observations to produce the analysis (superscript "*a*") state vector

$$\boldsymbol{w}_{\boldsymbol{k}}^{\boldsymbol{a}} = \boldsymbol{w}_{\boldsymbol{k}}^{\boldsymbol{f}} + \boldsymbol{w}_{\boldsymbol{k}}^{\boldsymbol{i}}, \quad (8)$$

where $\boldsymbol{w}_{\boldsymbol{k}}^{\boldsymbol{i}} = \boldsymbol{K}_{\boldsymbol{k}}(\boldsymbol{w}_{\boldsymbol{k}}^{\boldsymbol{o}} - \boldsymbol{H}_{\boldsymbol{K}}\boldsymbol{w}_{\boldsymbol{k}}^{\boldsymbol{f}})$ is the innovation vector, $\boldsymbol{K}_k$ is the Kalman gain matrix computed at each time step using a time evolving forecast error covariance matrix P^f given in Equations (9-10).

$$\boldsymbol{P}_{\boldsymbol{k}}{}^{\boldsymbol{f}} = \Psi_{\boldsymbol{k}-1}\boldsymbol{P}_{\boldsymbol{k}-1}^{\boldsymbol{a}}\Psi^{\boldsymbol{T}}{}_{\boldsymbol{k}-1} + \boldsymbol{Q}_{\boldsymbol{k}-1} \quad (9)$$

$$\boldsymbol{K}_{\boldsymbol{k}} = \boldsymbol{P}_{\boldsymbol{k}}^{\boldsymbol{f}}\boldsymbol{H}_{\boldsymbol{k}}^{\boldsymbol{T}}(\boldsymbol{H}_{\boldsymbol{k}}\boldsymbol{P}_{\boldsymbol{k}}^{\boldsymbol{f}}\boldsymbol{H}_{\boldsymbol{k}}^{\boldsymbol{T}} + \boldsymbol{R}_{\boldsymbol{k}})^{-1} \quad (10)$$

The error covariance matrix is also updated on the analysis step as

$$\boldsymbol{P}_{\boldsymbol{k}}^{\boldsymbol{a}} = (\boldsymbol{I} - \boldsymbol{K}_{\boldsymbol{k}}\boldsymbol{H}_{\boldsymbol{k}})\boldsymbol{P}_{\boldsymbol{k}}^{\boldsymbol{f}}. \quad (11)$$

The innovation vector shows how much additional information from the data will modify the model forecast in order to produce an optimal estimate of the state of the system. The value and the sign of the innovation vector depend on how much the observed and modeled values differ from each other, and on the estimated forecast and observational errors. For a detailed description of the Kalman filter algorithm see for example [*Ghil and Malone-Rizzoli,* 1991]. In the standard formulation of the Kalman filter, the model and observational error covariances matrices Q and R are assumed to be known. This rarely happens in practice and usually some simple approximations are made. In the current study the matrices Q and R are assumed to be diagonal and each of the diagonal elements are equal to 50% and 500 % of the modeled and observed PSD variance, respectively.

3.2 Reanalysis Results

By using information contained in the model matrix, sparse CRRES observations modify the PSD at all values of L at the time of updates, which are performed every hour of the simulation. Figure 3 top shows the result of the data assimilation with a radial diffusion model, which is usually referred to as "reanalysis" in atmospheric sciences [e.g. *Kalanay et al.,* 1996]. Since data at L*= 7 is not available for all times of the simulation we use the PSD L*=7 from the analysis step of the data assimilation as a boundary condition on the next forecast step. The boundary condition is modified by the data innovation even when data is not available. Figure 3 (middle) also shows the daily averaged CRRES data, for a direct comparison with the reanalysis. Note that unlike the simulations shown on Figure 2 the boundary condition is dynamically adjusted by the data and model as described above. Careful visual (subjective) analysis of the daily averaged values shows that for most of times daily averages are consistent with the reanalysis. However, the limited range of L-shells for which daily averages are available (and averaging over different parts of different orbits) complicates the analysis of the observations. As seen from Figure 3 peaks are formed when PSD is increasing, which clearly rules out the possibility of peaks being formed by the decrease at the outer boundary which can only decrease the PSD.

Figure 4 shows the 50-day averaged innovation vector from the analysis time step of the data assimilation (see Eq. (9)). It has a pronounced peak at L^*~5.5, indicating that observations are consistently adding PSD at this location in space. Presence of the peaks in the radial profile of the PSD may be explained by local acceleration driven by chorus waves operating near L^*~5.5, which is not accounted for by the radial diffusion model [e.g. *Varotsou et al.*, 2005], while negative values of the innovation vector at $L^*=7$ may be due to the losses to magnetopause and consequent outward radial diffusion [*Shprits et al.*, 2006b]. Other local processes such as acceleration by magnetosonic waves may also contribute to acceleration of electrons [*Horne, et al.*, 2007].

3.3 Profiles of PSD at different values of the invariant *K*

To verify that the effects of peaks in PSD produced by the local acceleration are observed at various values of pitch-angles and consequently at various values of *K* we repeated the analysis described in Section 3.2 for the three values of *K* of 0.025, 0.11, and 0.3 $G^{1/2}$ R_E. For a dipolar magnetic field three chosen values of *K* and fixed μ=700 MeV/G electrons' equatorial pitch-angles are approximately 70°, 50°, and 35° respectively (Figure 5). Assimilated PSD shows peaks around 5-6 R_E in all three cases (Figure 6). Peaks are stronger at higher *K* values, consistent with the observations of two case studies of the October 9 and August 26, 1990 [*Iles et al.*, 2006].

As suggested by *Iles et. al.* [2006] this effect could be due to the increase in energy with increasing K-value, or also could be due to a weaker radial diffusion rates at higher values of *K*. The result of the Kalman filtering are mostly controlled by the observations since the observational uncertainty is small compared to the estimated forecast error. Radial diffusion simply redistributes PSD, which is mostly determined on the analysis step by the data. Even though the radial diffusion rates are independent of the pitch-angle in our model, the pitch-angle dependence is produced by the data innovation.

The similarity in the spatial and temporal patterns of the PSD at different values of *K* shows that local acceleration is effective for a range of energies. It also indicates that pitch-angle diffusion is fast enough to transport particles in pitch-angle and establish equilibrium shapes of the pitch-angle distributions which increase and decay as a whole. Such behavior is similar to the recent results of the pitch-angle and energy scattering simulations [*Shprits et al.*, 2006c].

3.4 PSD for various values of the magnetic moment μ

Figure 7 shows the change in energy of electrons in the dipolar field, diffusing radially and conserving the first and the second adiabatic invariants for K=0.11 $G^{1/2}$ R_E and relatively small values of μ=550 MeV/G and μ=700 MeV/G. For a fixed value of *K*, particles with higher value of the first adiabatic invariant have higher kinetic energy. The location of the peaks in data assimilation results (Figure 8) as well as times at which peaks are formed and decay are similar. However, in the case of higher magnetic moments the PSD peaks are more pronounced. This result is also consistent with theoretical estimates of the effect of the competition of acceleration and loss. Scattering losses produced by chorus waves dominate over acceleration for electrons at energies below ~ 300-500 keV, while above 1 MeV chorus waves produce net acceleration [*Horne, et al.*, 2006; *Li et al.*, 2007]. At lower energies the net acceleration is weaker and should produce more monotonic profiles of PSD, which can explain the observed strengthening of the peaks with increasing magnetic moment.

4. Identical twins experiments (Simulations with synthetic data)

If the model used for the simulations consistently underestimates observations, and measurements are confined to a limited range of L-shell, the observational data will increase the PSD at the locations where data is available and may produce artificial peaks in PSD. To verify that the peaks are not a result of the limitations in data coverage we conducted numerical experiments with so-called “synthetic data”. Such tests are also commonly referred to as “identical twin experiments” and are performed to verify the robustness of the method. In the identical twin experiments, model simulations with a given set of parameters are performed to produce “synthetic data” which is used as a source of artificial observational data for the subsequent data assimilation numerical experiments.

For our first identical twin experiments we initially performed the radial diffusion simulation with a lifetime τ parameterized as 5/Kp (Figure 9 top). By taking only points for which CRRES observations are available we create a synthetic sparse data set (Figure 9 second panel). This data is assimilated with the radial diffusion model for which lifetime is parameterized as 1/Kp. The results of the model simulations without data assimilation are shown on Figure 9 (third panel). We choose the parameters of the model so that our artificially produced data overestimates model results. This allows us to verify that data assimilation is capable of reproducing a general structure of the underlying PSD even when the data is sparse. In the identical twin experiment the underlying structure of PSD is is known, in our case monotonic profile of the PSD.

The results of the data assimilation show that the reconstructed PSD ,(Figure 9, forth panel) even when artificial data overestimates the model results, captures monotonic profiles of the underlying PSD. The model with data assimilation quite accurately reproduces synthetic data at L>5 where observations, even though sparse, are available, but fails to reproduce the PSD at lower L-shells where no data is available. At lower L-values the dynamics of the radiation belts fluxes will depend on the competition between local acceleration and loss processes and can not be accurately determined using only observations at higher L-shells.

Figure 10 shows the results of the identical twin experiments with synthetic data which underestimates the model results . As in the previous case, the model with data assimilation is able to reproduce the underlining structure (monotonic profile of PSD) and reproduces quite well values of the synthetic data at higher L-shells, but fails to reproduce synthetic data at lower L-shells, where no synthetic data is available.

Figure 11 shows the averaged innovation vector for the identical twin experiments described above. The innovation vector is positive when the data overestimates the model results (the lifetime used for the synthetic data is longer than for the physical model) and negative when data underestimats observations. Unlike in the case of simulations with CRRES data, the innovation vector is monotonic at all L-values for which data is available, (compare with Figure 4). This shows that peaks of the PSD shown on Figures 3,6 and 8 are not produced by the limitations in the data coverage, but instead reflect information contained in the underlying PSD observations.

5 Discussion

In this study we show how data assimilation using a Kalman filter may be applied to reconstruct PSD (perform reanalysis) for a sparse data set. We used a relatively crude 1D radial diffusion model, which has significant "errors", on the scale of a few hundred percent. The term "error" conventionally used in the description of the Kalman filter actually results from a physical limitation of the models. These limitations can be incorporated into the data assimilation algorithms by assigning an "error" and allowing the model to be adjusted to assimilated data. Since we have a rather inaccurate model, we specify model and observational errors such that data points have more weight in the analysis step than the information provided by the model. In this case data assimilation can be considered as a smart interpolation algorithm, which reconstructs observations using a transport model at all radial locations with a high time resolution. Even with a simple physical model and a very sparse data we are able to objectively reconstruct PSD and study the dynamical evolution of its radial profiles. We also show that at each L-shell, radiation belt dynamics are strongly influenced by the local processes, and that observations at all L-shells are required to constrain the model solutions. This has important implications for the design of future missions and choice of the future satellite orbits and future improvements of the models.

However the capabilities of data assimilation, can go far beyond that. Data assimilation can be used to combine model and data from different satellites and instruments, which may have different observational errors to simulate the global evolution of radiation belt fluxes. The reanalysis of data from multiple spacecraft may result in a significant reduction of the error of the analysis, compared to the errors of each of the satellites or instruments. Observational errors for each satellite can be specified so that data from more accurate instruments has more weight on the analysis step, while even quite inaccurate measurements can still contribute to the final reanalysis data product.

Application of the Kalman filter to a 3D model, which takes into account radial diffusion, pitch-angle scattering, and local acceleration, will provide even further improvement to assimilation techniques. Such 3D models can potentially account for more physical processes and can also use the knowledge of the dynamics of pitch-angle distributions and energy spectrum which will allow to utilize a vast array of available measurements.

Inter-calibration of the satellites is conventionally performed using satellite conjunctions (measurements of the same variables on a given flux tube [e.g. *Friedel et al*., 2005]). Differences in the instrument parameters, the range of measured pitch-angles and energies, and differences in the orbital properties usually limit the number of available conjunctions. With new magnetic field models and more data available from multiple satellites new inter-calibration techniques based on comparison of PSD on a magnetic drift shell offer some additional, but still limited, inter-calibration opportunities [*Chen et al*., 2005]). Data assimilation offers another, more flexible and robust, way to study the errors of various space instruments and inter-calibrate them. By using a reanalysis based on the different satellites we may compare the observational errors and correct for systematic errors. Comparison of reanalysis data products, which are produced with a different set of instruments, will not be limited to conjunction points and will be available at all times. Results of the reanalysis may be also used for statistical studies and creation of the empirical models [*e.g. Vassiliadis et al*., 2003, 2005; *Kondrashov et al.*, 2005].

6. Conclusions

In this study we have performed reanalysis of the PSD for the set of fixed values of adiabatic invariants μ and K using the radial diffusion model. We show that at μ=700 MeV/G and K=0.11 $G^{0.5}$ radial profiles frequently exhibit peaks in PSD which can not be produced by the variation in the outer boundary and may thus be only explained as a result of local acceleration of electrons. The peak of the innovation vector is located approximately at L=5.5 indicating the location of the local acceleration source. Reanalysis of the phase space densities at different values of K of 0.025, 0.11 and 0.3 $G^{1/2}$ R_E shows that peaks are present at the same times at various pitch-angles, but are stronger at higher values of K (smaller pitch-angles). Peaks at lower values of μ (500 MeV/G) are also less pronounced, most likely due to energy dependence of the local acceleration and loss. Using synthetic data we show that sparse CRRES MEA data is sufficient for reconstructing the PSD with high resolution in time and space using the Kalman filter.

Appendix A: Adiabatic Invariants and PSD calculations

First adiabatic invariant associate with a gyro-motion of a particle in the guiding center reference frame may be expressed as :

$$\mu = \frac{\boldsymbol{p}_{\perp}^{2}}{2\boldsymbol{m}_0\boldsymbol{B}} \qquad \text{(A1)}$$

where p is the relativistic momentum in the direction perpendicular to the direction of the magnetic field, m_0 is the electron rest mass and, B is the magnitude of the local magnetic field. Second adiabatic invariant associated with bounce motion may be expressed as:

$$J = \int_{bounce} p_{\|} ds = 2\sqrt{2\,\mu\, m_0} \int_{S_m}^{S_m^{'}} \sqrt{B_m - B(s)}\, ds \qquad \text{(A2)}$$

where $p_{||}$ is the relativistic momentum in the direction parallel to the direction of magnetic field, B_m is a field strength at the mirror point, S_m and $S^{'}_m$ are the distancies along the field line from the equator to the mirror point and *ds* is the distance element along the field line.

K-invariant is a combination of the first two invariants which is independent on the particle mass and charge is usually expressed as:

$$K = \frac{J}{2\sqrt{2\mu}} = \int_{S_m}^{S_m^{'}} \sqrt{B_m - B(s)}\, ds \qquad \text{(A3)}$$

The conservation of the 3rd adiabatic invariant represents the conservation of the magnetic flux through the drifting orbit around the Earth of the electron.

$$\Phi = \int_{drift} B dS \qquad \text{(A4)}$$

The Roederer parameter L^* is commonly used instead of Φ where M is the Earth magnetic moment.

$$L^* = \frac{2\pi M}{\Phi R_E} \qquad \text{(A5)}$$

At any L-shell PSD f may be related to the differential flux as [Rossi and Olbert, 1970]

$$f = \frac{10^3}{2.9979 \cdot 10^{10}} \frac{j}{p^2 c^2}$$

Where j is the differential flux in units of $(\text{ sr s cm}^2 \text{ keV})^{-1}$, pc is in units of MeV and PSD is in $(\text{MeV/c cm})^{-3}$.

Acknowledgements

This research was supported by the NASA LWS grants NNX06AB84G and NNG04GN44G and IGPP Los Alamos Mini Grant. Work at Los Alamos was supported by the U.S. Department of Energy DREAM project.

References

Bourdarie, S., D. Boscher, T. Beutier, J.-A. Sauvaud, M. Blanc (1996), Magnetic storm modeling in the Earth's electron belt by the Salammbo code, *J. Geophys. Res., 101*, 27171-27176, 10.1029/96JA02284.

Bourdarie, S., D. Boscher, T. Beutier, J.-A. Sauvaud, M. Blanc (1996), Magnetic storm modeling in the Earth's electron belt by the Salammbo code, *J. Geophys. Res., 101*, 27171-27176, 10.1029/96JA02284.

Brautigam, D. H., and J. M. Albert (2000), Radial diffusion analysis of outer radiation belt electrons during the October 9, 1990, magnetic storm, *J. Geophys. Res.*, *105*, 291-310.

Chen, Y., R. Friedel, G. Reeves, T. Onsager, and M. Thomsen (2005), Multi-satellite determination of the relativistic electron PSD at the geosynchronous orbit: Methodology and initial results in magnetic quiet times, *J. Geophys. Res.*, *110,* A10210, doi:10.1029/2004JA010895.

Chen Y., R. H. W. Friedel, G. D. Reeves (2006), PSD distributions of energetic electrons in the outer radiation belt during two Geospace Environment Modeling Inner Magnetosphere/Storms selected storms, *J. Geophys. Res., 111*, A11S04, doi:10.1029/2006JA011703.

Friedel, R. H. W. , S. Bourdarie, J. F. Fennell, S. Kankeal, and T. E. Cayton (2003), “Nudging” the Salammbo code: First results of seeding a diffusive radiation belt code with in situ data: GPS GEO, HEO, and POLAR, *Eos Trans. AGU*, 84(46) Fall Meet. Suppl., Abstract SM11D-06.

Friedel, R. H. W., et al. (2005), Intercalibration of magnetospheric energetic electron data, *Space Weather*, *3, S09B04, doi:10.1029/2005SW000153.*

Ghil, M., and P. Malanotte-Rizzoli (1991), Data assimilation in meteorology and oceanography. *Adv. Geophys.*, *33*, 141–266.

Green, J. C., and M. G. Kivelson (2004), Relativistic electrons in the outer radiation belt: Differentiating between acceleration mechanisms, *J. Geophys. Res.*, *109*, A03213, doi:10.1029/2003JA010153.

Horne, R. B., R. M. Thorne, S. A. Glauert, J. M. Albert, N. P. Meredith, and R. R. Anderson (2005a), Timescales for radiation belt electron acceleration by whistler mode chorus waves, *J. Geophys. Res.*, *111*, A03225, doi:10.1029/2004JA010811.

Horne, R. B. R. M. Thorne , Y. Y. Shprits , N. Meredith , S. Glauert , A. Smith , S. Kanekal, D. Baker , M. Engebretson , J. Posch , M. Spasojevic , U. Inan , J. Pickett, P. Décréau (2005b), Wave acceleration of electrons in the Van Allen radiation belts, *Nature*, *437*, 227–230, doi:10.1038/nature03939.

Horne, R. B., R. M. Thorne, S. A. Glauert, N. P. Meredith, D. Pokhotelov, and O. Santolik (2007), Electron acceleration in the Van Allen belts by fast magnetosonic waves, *Geophys. Res. Lett.*, in press.

Iles, R. H. A., N. P. Meredith, A. N. Fazakerley, and R. B. Horne (2006), Phase space density analysis of the outer radiation belt energetic electron dynamics, *J. Geophys. Res.*, *111*, A03204, doi:10.1029/2005JA011206.

Kalman, R. E. (1960), A new Approach to Linear Filtering and Prediction Problems”, Transaction of the ASME –*Journal of Basic Engineering*, 35-45.

Kalnay, E. et al. (1996), The NCEP/NCAR 40-year reanalysis project, *Bull. Amer. Met. Soc.*, 77, 437-471.

Kondrashov, D., Y. Shprits, M. Ghil and R. Thorne (2007), A Kalman Filter Technique to Estimate Relativistic Eelectron Lifetimes in the Outer Radiation Belt, *J. Geophys. Res,* accepeted.

Kondrashov, D., S. Kravtsov, A. W. Robertson, and M. Ghil (2005), A hierarchy of data-based ENSO models, *J. Climate*, *18*, 4425–4444.

Li, W, Y. Y. Shprits, and R. M. Thorne (2007), Dynamic evolution of energetic outer zone electrons due to wave-particle interactions during storms, submitted to *J. Geophys. Res.*

Mathie, R. A., and I. R. Mann (2000), A correlation between extended intervals of ULF wave power and storm-time geosynchronous relativistic electron flux enhancements, *Geophys. Res. Lett.*, *27*, 3261.

Meredith, N. P., R. B. Horne, R. R. Anderson (2001), Substorm dependence of chorus amplitudes: Implications for the acceleration of electrons to relativistic energies, *J. Geophys. Res.*, *106*(A7), 13165-13178, 10.1029/2000JA900156.

Meredith N. P., R. B. Horne, R. H. A. Iles, R. M. Thorne, D. Heynderickx, and R. R. Anderson, (2002), Outer zone relativistic electron acceleration associated with substorm-enhanced whistler mode chorus, *J. Geophys. Res.*, *107* (A7), doi:10.1029/2001JA900146.

Miyoshi Y., A. Morioka, T. Obara, H. Misawa, T. Nagai, and Y. Kasahara, Rebuilding process of the outer radiation belt during the 3 November 1993 magnetic storm: NOAA and Exos-D observations, *J. Geophys. Res., 108* (A1), 1004, doi:10.1029/2001JA007542, 2003.

Naehr S. M. and F. R. Toffoletto (2005), Radiation belt data assimilation with an extended Kalman filter, *Space Weather, 3*, S06001, doi:10.1029/2004SW000121.

Perry K. L., M. K. Hudson, S. R. Elkington (2005), Incorporating spectral characteristics of Pc5 waves into three-dimensional radiation belt modeling and the diffusion of relativistic electrons, *J. Geophys. Res., 110,* A03215, doi:10.1029/2004JA010760.

Reeves G. D., K. L. McAdams, R. H. W. Friedel, T. P. O'Brien (2003), Acceleration and loss of relativistic electrons during geomagnetic storms, Geophys. Res. Lett., 30 (10), 1529, doi:10.1029/2002GL016513.

Rossi, B., and S. Olbert (1970), *Introduction to the Physics of Space,* McGraw Hill, New York.

Selesnick, R. S., and J. B. Blake (2000), On the source location of radiation belt relativistic electrons, *J. Geophys. Res.*, *105,* 2607.

Schulz, M., and L. Lanzerotti, *Particle Diffusion in the Radiation Belts,* Spinger, New York ,1974.

Shprits, Y. Y., and R. M. Thorne (2004), Time dependent radial diffusion modeling of relativistic electrons with realistic loss rates, *Geophys. Res. Lett.*, *31*, L08805, doi:10.1029/2004GL019591.

Shprits, Y. Y., R. M. Thorne, G. D. Reeves, and R. Friedel (2005), Radial diffusion modeling with empirical lifetimes: Comparison with CRRES observations, *Ann. Geophys.*, *23*, 1467–1471.

Shprits, Y. Y., R. M. Thorne, R. B. Horne, S. A. Glauert, M. Cartwright, C. T. Russell, D.

N. Baker, and S. G. Kanekal (2006a), Acceleration mechanism responsible for the formation of the new radiation belt during the 2003 Halloween solar storm, *Geophys. Res. Lett., 33*, L05104, doi:10.1029/2005GL024256.

Shprits, Y. Y., R. M. Thorne, R. Friedel, G. D. Reeves, J. F. Fennell, D. Baker, and S. G. Kanekal (2006b), Outward radial diffusion driven by losses at magnetopause, *J. Geophys. Res., 111*, A11214, doi:10.1029/ 2006JA011657.

Shprits, Y. Y., W. Li, and R. M. Thorne (2006c), Controlling effect of the pitch angle scattering rates near the edge of the loss cone on electron lifetimes, *J. Geophys. Res., 111*, A12206, doi:10.1029/2006JA011758.

Sun CJ, Hao Z, Ghil M, et al.Data assimilation for a coupled ocean-atmosphere model. Part I: Sequential state estimation, Monthly Weather Rev. 130 (5): 1073-1099 2002

Tsyganenko, M. and D. Stern (1996), Modeling the global magnetic field the large-scale Birkeland current system, *J. Geophys. Res.*, *101*, 187–27,198.**[**

Vampola, A.L., Osborne, J.V., Johnson, B.M. (1992), CRRES magnetic electron spectrometer AFGL-701-5A (MEA*). Journal of Spacecr. Rockets 29*, 592-594.

Varotsou, A., D. Boscher, S. Bourdarie, R. B. Horne, S. A. Glauert, and N. P. Meredith (2005), Simulation of the outer radiation belt electrons near geosynchronous orbit including both radial diffusion and resonant interaction with Whistler-mode chorus waves, *Geophys. Res. Lett.*, *32*, L19106, doi:10.1029/2005GL023282.

Vassiliadis D., A. J. Klimas, R. S. Weigel, D. N. Baker, E. J. Rigler, S. G. Kanekal, T. Nagai, S. F. Fung, R. W. H. Friedel, T. E. Cayton (2003), Structure of Earth's outer radiation belt inferred from long-term electron flux dynamics, *Geophys. Res. Lett., 30* (19), 2015, doi:10.1029/2003GL017328.

Vassiliadis D., S. F. Fung, A. J. Klimas (2005), Solar, interplanetary, and magnetospheric parameters for the radiation belt energetic electron flux, *J. Geophys. Res.*, *110,* A04201, doi:10.1029/2004JA010443.

Figure 1 Dependence of the equatorial pitch-angle and kinetic energy on L-shell for fixed values of K=0.11 $G^{0.5}$ R_E and μ=700 MeV/G.

Figure 2. (Top) Hourly averaged PSD inferred from CRRES MEA observations using T98 Magnetic field model for K=0.11 $G^{0.5}$ R_E and μ=700 MeV/G for 50 day period starting on August 18, 1990. (Middle) Results of the radial diffusion simulations with constant outer boundary conditions and lifetime parameterized at 5/Kp. (Bottom) Evolution of the Kp index used for the radial diffusion simulations. PSD is given in units of $\log_{10}(c/MeV/cm)^3$*1e6).

Figure 3. (Top) Results of the data assimilation with hourly-averaged CRRES MEA data and a radial diffusion model for a 50 day period starting on August 18, 1990. (Middle) Daily averaged CRRES MEA fluxes. (Bottom) Evolution of the Kp index used for simulations. PSD is given as in units of $\log10(c/MeV/cm)^3$*1e6).

Figure 4. 50-day averaged innovation vector as a percentage of the average value of the PSD at a given L-shell.

Figure 5 Dependence of the equatorial pitch-angle and kinetic energy on L-shell for a fixed value of μ=700 MeV/G. and various values of K=0.025, 0.11, and 0.3 $G^{1/2} R_E$.

Figure 6 PSD at for a fixed magnetic moment μ=700 MeV/ G and for K values of 0.025, 0.11 and 0.3 $G^{1/2}$ R_E for 50 day period starting on August 18, 1990.. PSD is given as in units of $\log10(c/MeV/cm)^3$*1e6).

Figure 7 Dependence of the kinetic energy on L-shell for fixed μ=550 MeV/G (left) amd μ=700 MeV/G (right) with K= 0.11 $G^{1/2} R_E$ for both cases.

Figure 8 PSD at μ=550 and 700 MeV/G for a 50 day period starting on August 18, 1990. PSD is given in units of $\log_{10}(c/MeV/cm)^3*1e6$).

Figure 9. Results of the identical twin experiment. (First panel) Results of the radial diffusion code with a lifetime parameter τ set to 5/Kp. (Second panel) Sparse data produced by flying a virtual CRRES satellite through the synthetic data as shown on in the first panel. (Third panel). Results of the simulations with the radial diffusion model with τ=5/Kp, used as a physics based model for the identical twin experiment. (Fourth panel) Reanalysis of the synthetic data. (Bottom) Evolution of the Kp index used for the simulations. PSD is given as in units of log10$(c/MeV/cm)^3*1e6$).

Figure 10. Same as Figure 9 but with data produced with parameter τ=1/Kp and model with parameter τ=5/Kp.

Figure 11. The 50-day averaged innovation vector as a percentage of the average value of the PSD at a given L-shell for the identical twin experiments shown on Figure 9 and Figure 10.

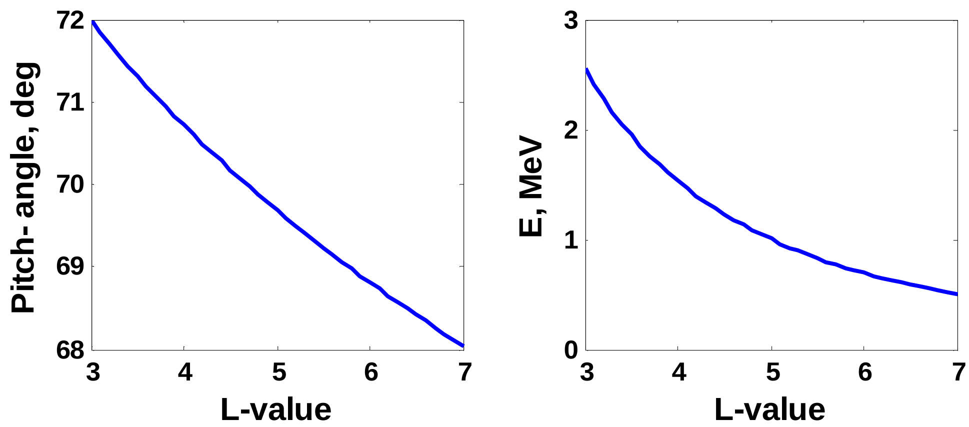

Figure 1 Dependence of the equatorial pitch-angle and kinetic energy on L-shell for fixed values of K=0.11 $G^{0.5}$ R_E and μ=700 MeV/G.

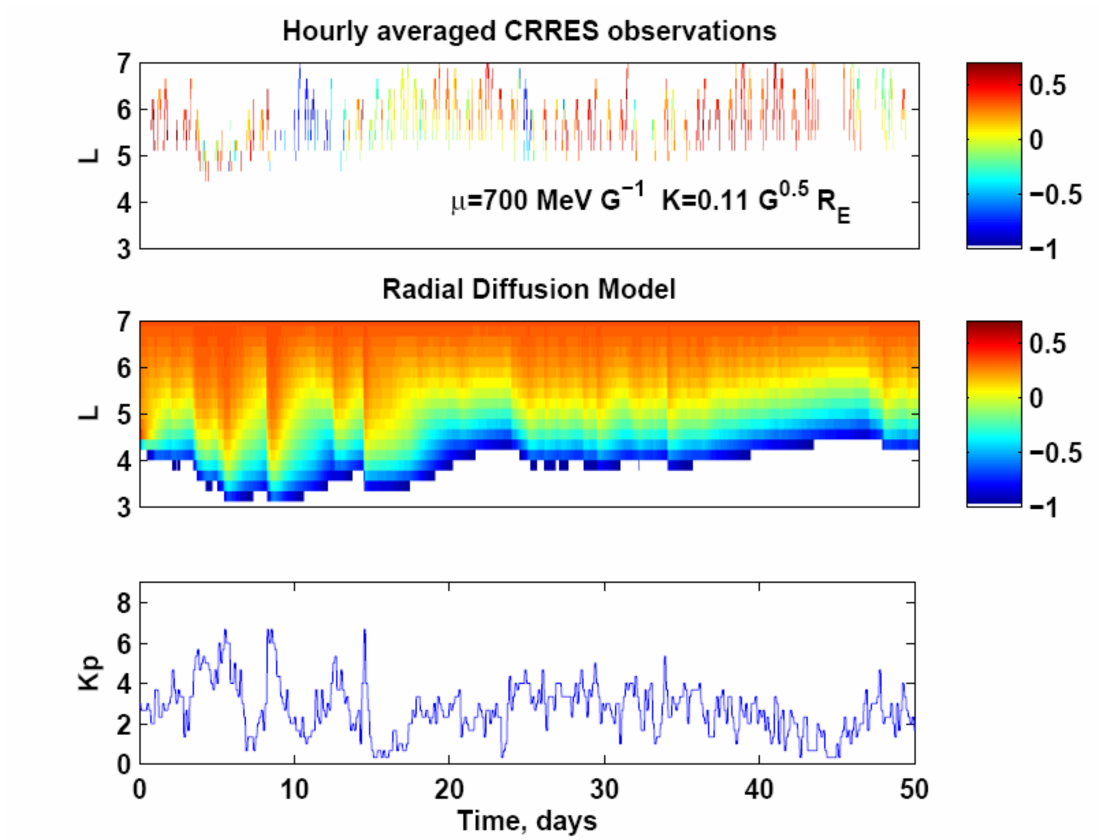

Figure 2. (Top) Hourly averaged PSD inferred from CRRES MEA observations using T98 Magnetic field model for K=0.11 $G^{0.5}$ R_E and μ=700 MeV/G for 50 day period starting on August 18, 1990. (Middle) Results of the radial diffusion simulations with constant outer boundary conditions and lifetime parameterized at 5/Kp. (Bottom) Evolution of the Kp index used for the radial diffusion simulations. PSD is given in units of $\log_{10}(c/MeV/cm)^3$*1e6).

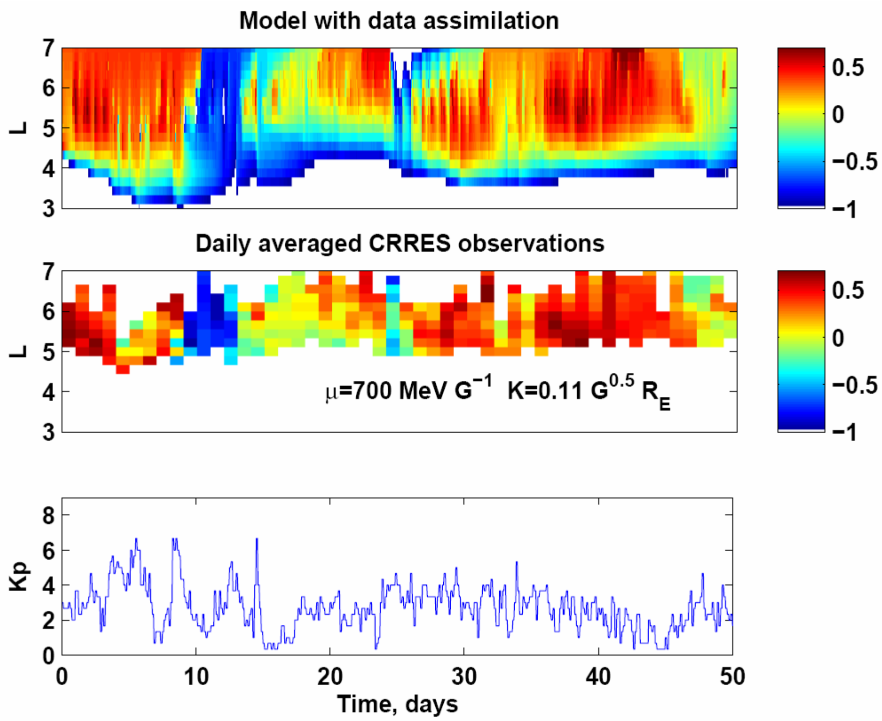

Figure 3. (Top) Results of the data assimilation with hourly-averaged CRRES MEA data and a radial diffusion model for a 50 day period starting on August 18, 1990. (Middle) Daily averaged CRRES MEA fluxes. (Bottom) Evolution of the Kp index used for simulations. PSD is given as in units of log10(c/MeV/cm)^3*1e6).

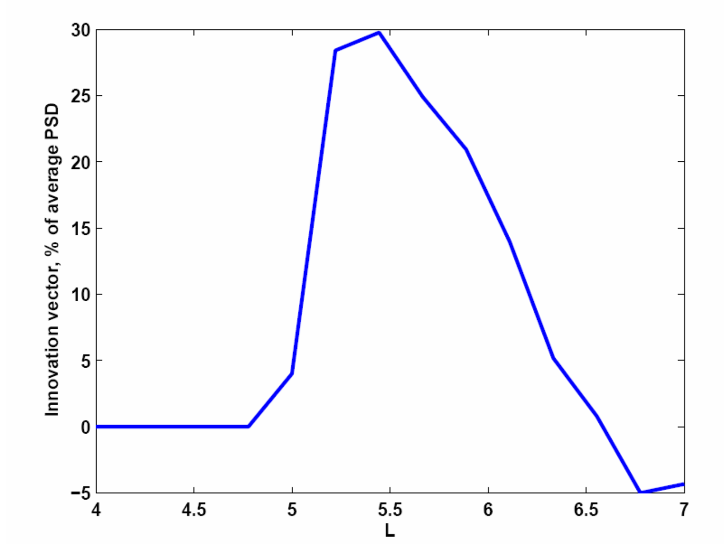

Figure 4. The 50-day averaged innovation vector as a percentage of the average value of the PSD at a given L-shell.

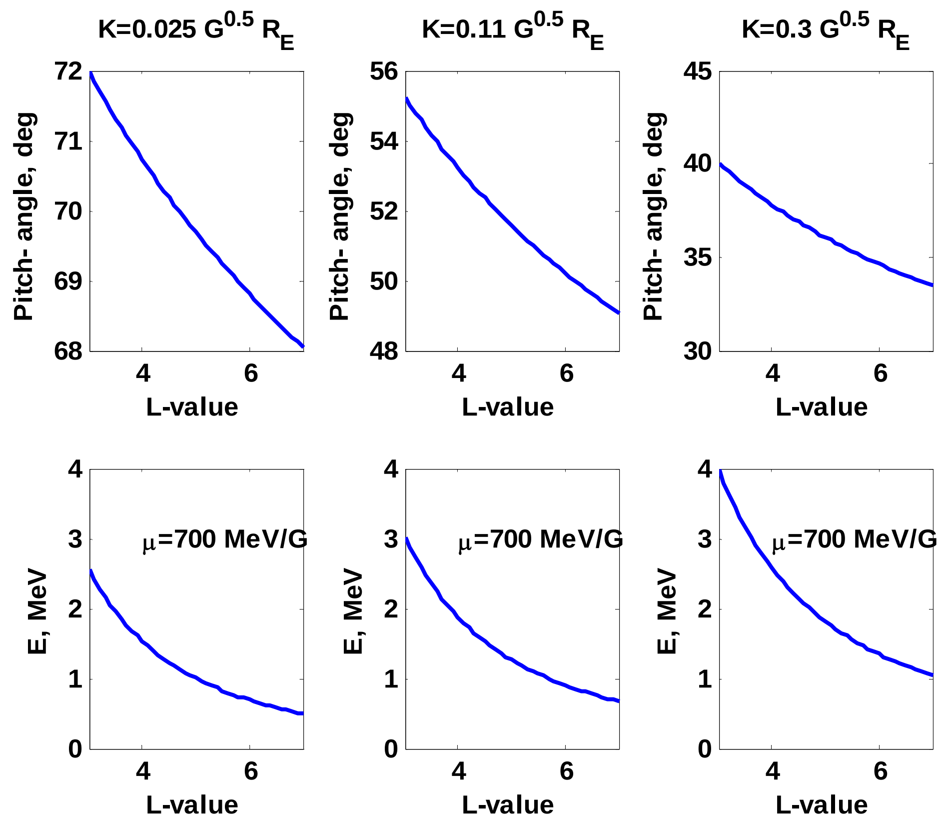

Figure 5 Dependence of the equatorial pitch-angle and kinetic energy on L-shell for a fixed value of μ=700 MeV/G and various values of K=0.025, 0.11, and 0.3 G $^{1/2}R_E$ assuming a dipolar magnetic field.

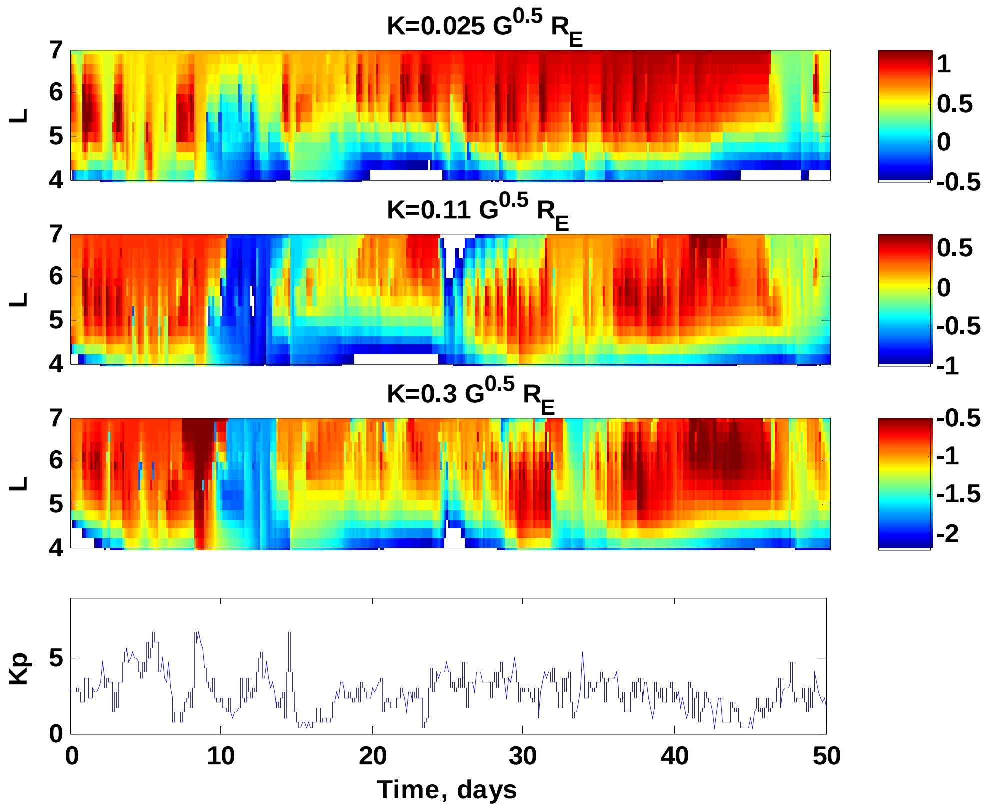

Figure 6 PSD at for a fixed magnetic moment μ=700 MeV/ G and for *K* values of 0.025, 0.11 and 0.3 $G^{1/2}$ R_E for 50 day period starting on August 18, 1990.. PSD is given as in units of log10(c/MeV/cm)^3*1e6).

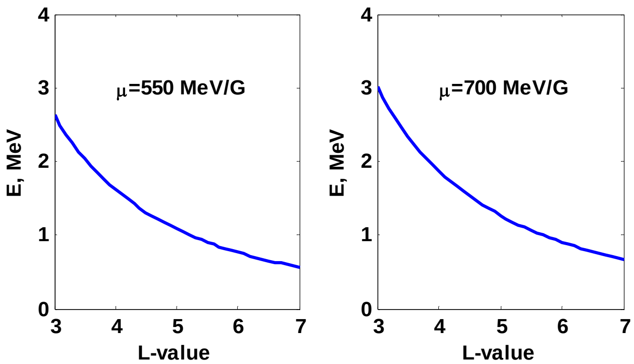

Figure 7 Dependence of the kinetic energy on L-shell for fixed μ=550 MeV/G (left) and μ=700 MeV/G (right) assuming a dipolar magnetic field with K= 0.11 G $^{1/2}R_E$ for both cases.

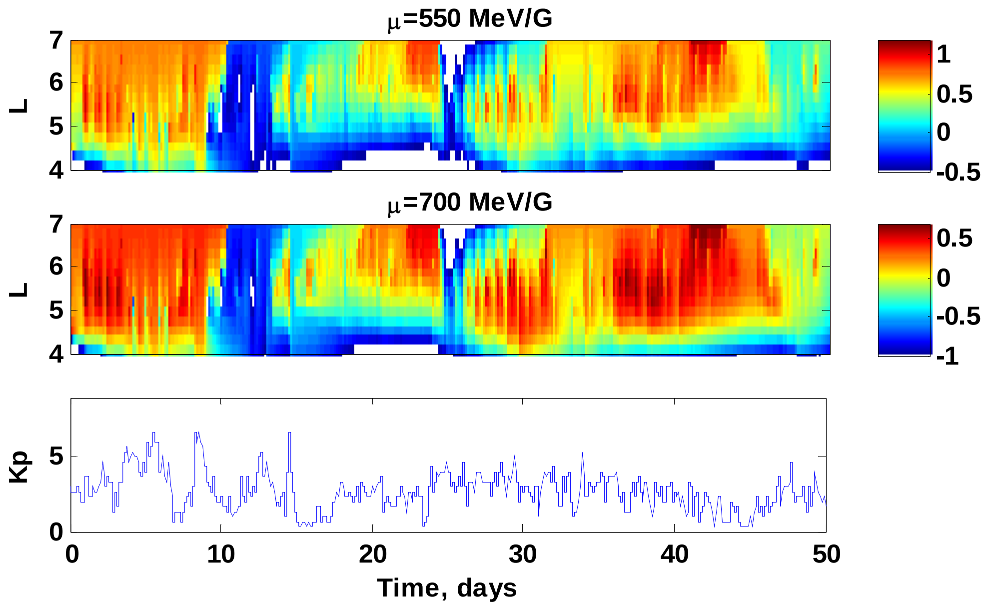

Figure 8 PSD at μ=550 and 700 MeV/G for a 50 day period starting on August 18, 1990. PSD is given in units of $\log_{10}(c/MeV/cm)^3*1e6$).

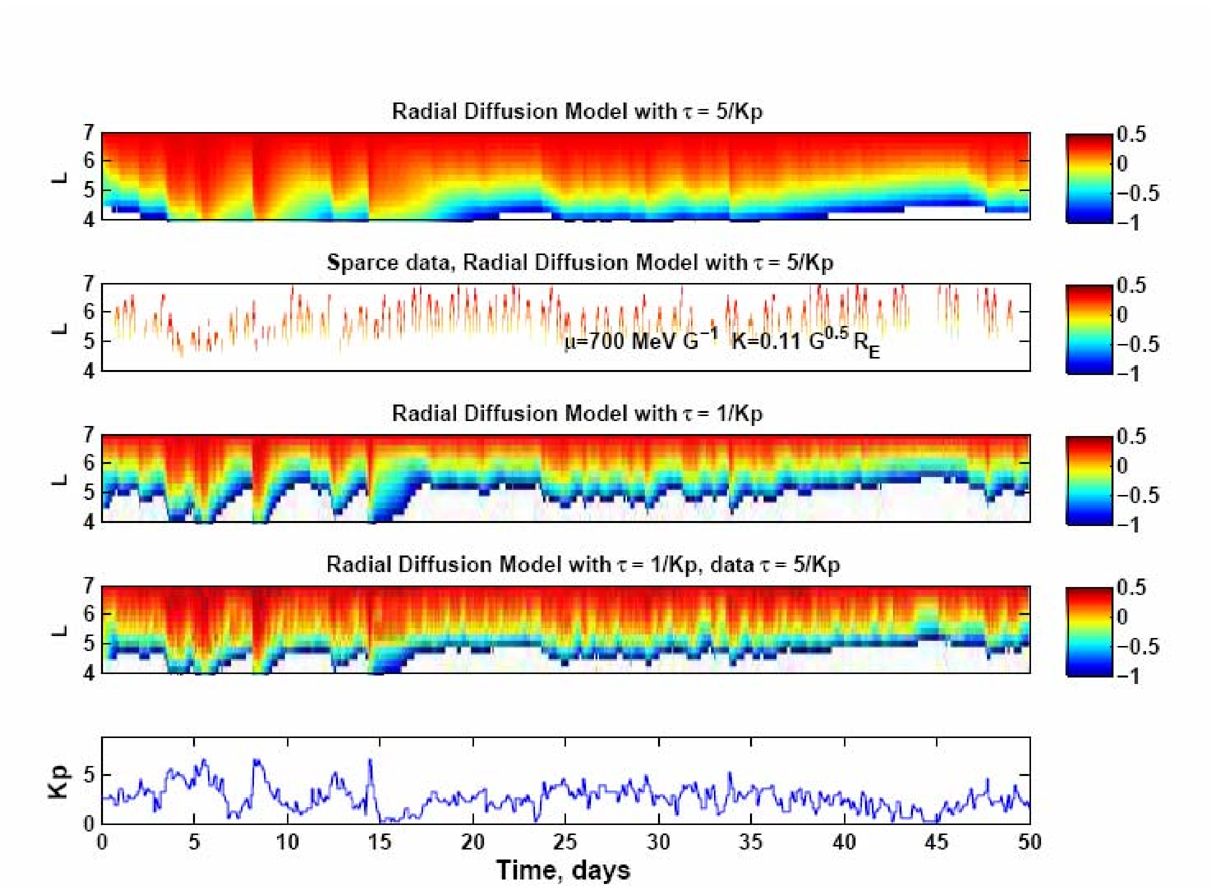

Figure 9. Results of the identical twin experiment. (First panel) Results of the radial diffusion code with a lifetime parameter τ set to 5/Kp. (Second panel) Sparse data produced by flying a virtual CRRES satellite through the synthetic data as shown on in the first panel. (Third panel) Results of the simulations with the radial diffusion model with τ=1/Kp, used as a physics based model for the identical twin experiment. (Fourth panel) Reanalysis of the synthetic data. (Bottom) Evolution of the Kp index used for the simulations. PSD is given as in units of log10(c/MeV/cm)^3*1e6).

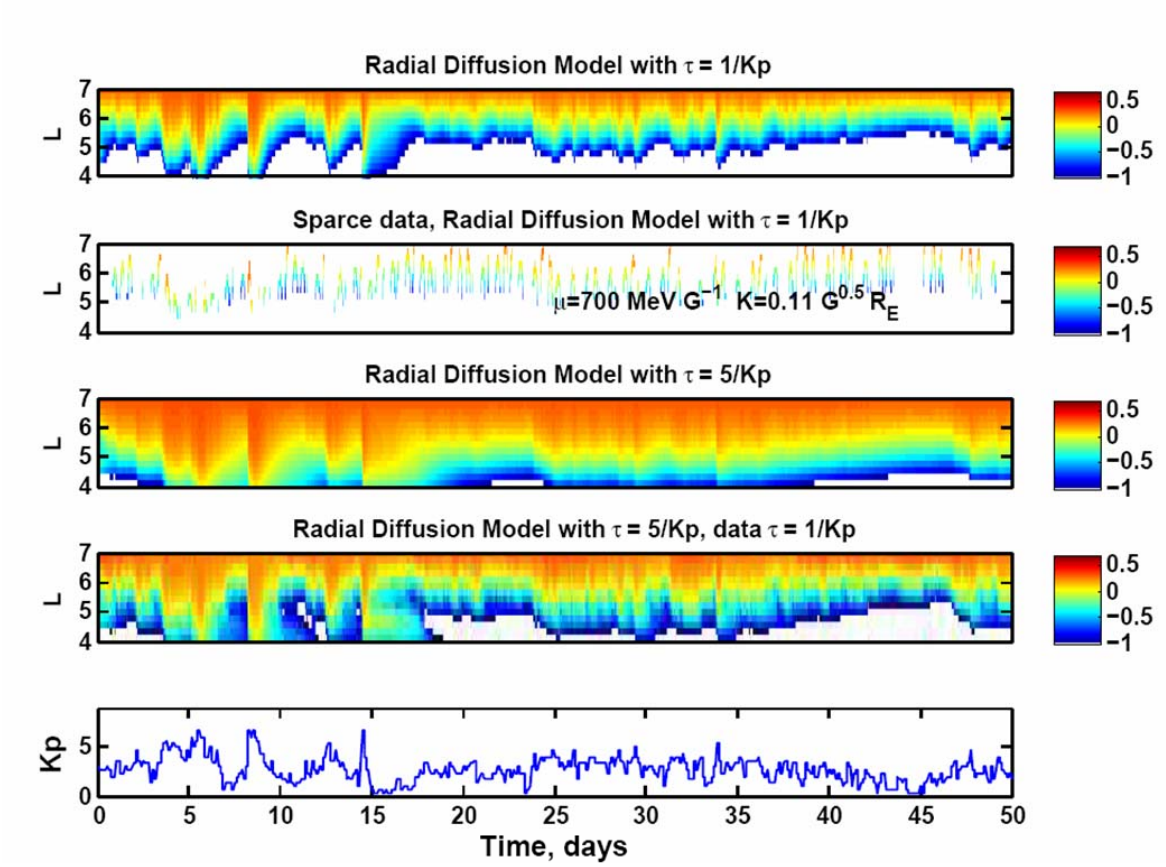

Figure 10. Same as Figure 9 but with data produced with parameter τ=1/Kp and model with parameter τ=5/Kp.

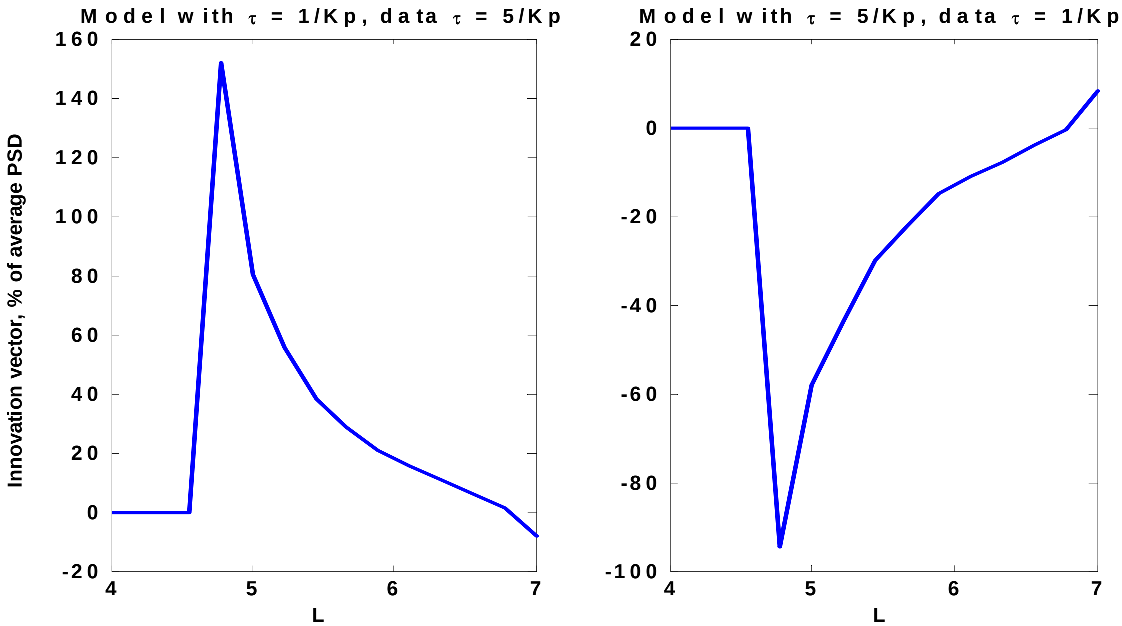

Figure 11. The 50-day averaged innovation vector as a percentage of the average value of the PSD at a given L-shell for the identical twin experiments shown on Figure 9 and Figure 10.